UNIVERSITY *of* York

This is a repository copy of *Monitoring Base Specific Dynamics during Melting of DNA-Ligand Complexes using Temperature-Jump Time-Resolved Infrared Spectroscopy*.

White Rose
university consortium
Universities of Leeds, Sheffield & York

eprints@whiterose.ac.uk
https://eprints.whiterose.ac.uk/

Monitoring Base-Specific Dynamics during Melting of DNA−Ligand Complexes Using Temperature-Jump Time-Resolved Infrared Spectroscopy

Robby Fritzsch,[†] Gregory M. Greetham,[‡] Ian P. Clark,[‡] Lucy Minnes,[†] Michael Towrie,[‡] Anthony W. Parker,[‡] and Neil T. Hunt[*,§]

[†]Department of Physics, SUPA, University of Strathclyde, Glasgow G4 0NG, U.K.

[‡]STFC Central Laser Facility, Research Complex at Harwell, Rutherford Appleton Laboratory, Harwell Campus, Didcot OX11 0QX, U.K.

[§]Department of Chemistry and York Biomedical Research Institute, University of York, Heslington, York YO10 5DD, U.K.

Ⓢ *Supporting Information*

ABSTRACT: Ultrafast time-resolved infrared spectroscopy employing nanosecond temperature-jump initiation has been used to study the melting of double-stranded (ds)DNA oligomers in the presence and absence of minor groove-binding ligand Hoechst 33258. Ligand binding to ds(5′-GCAAATTTCC-3′), which binds Hoechst 33258 in the central A-tract region with nanomolar affinity, causes a dramatic increase in the timescales for strand melting from 30 to ∼250 μs. Ligand binding also suppresses premelting disruption of the dsDNA structure, which takes place on 100 ns timescales and includes end-fraying. In contrast, ligand binding to the ds(5′-GCATATATCC-3′) sequence, which exhibits an order of magnitude lower affinity for Hoechst 33258 than the A-tract motif, leads to an increase by only a factor of 5 in melting timescales and reduced suppression of premelting sequence perturbation and end-fraying. These results demonstrate a dynamic impact of the minor groove ligand on the dsDNA structure that correlates with binding strength and thermodynamic stabilization of the duplex. Moreover, the ability of the ligand to influence base pairs distant from the binding site has potential implications for allosteric communication mechanisms in dsDNA.
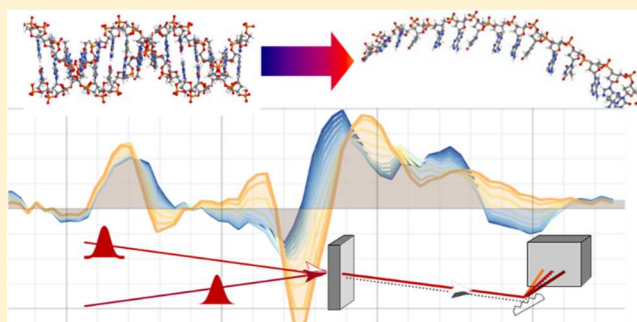
INTRODUCTION

Double-stranded deoxyribonucleic acid (dsDNA) acts as a repository for genetic information but only becomes biologically active, for example, when participating in transcription and replication, following partial unwinding of the duplex structure. This means that structural dynamics of dsDNA are crucial to its cellular function and form an essential part of the process of recognition and selective DNA binding.

In a chemical biology context, molecular recognition of dsDNA by small molecule ligands enables the location of functional groups on DNA architectures for nanotechnological applications, while selective local stabilization of the DNA duplex structure facilitates external modulation of biological function, providing viable platforms for the design of gene therapy techniques.[1−7] Despite the fundamental nature of DNA recognition and binding, the molecular details underpinning strong and specific interactions with DNA are not fully understood.[8] Strong ligand binding is often accompanied by an elevated DNA melting temperature even when binding is mediated by noncovalent interactions between the ligand and DNA. While the thermodynamic implications of this stabilization are clear, the underlying molecular mechanism is not

known, although computational simulations have suggested that the origin may lie in alteration of DNA strand dynamics.[9]

There is thus a need to observe and understand DNA dynamics, but the dsDNA macromolecule undergoes perturbations in structure that arise from both inter and intramolecular processes that span a wide range of timescales. Ultrafast dynamics have been linked to water motion[10] and solvation interactions,[11,12] both within the grooves of dsDNA and between phosphate groups and the surrounding solvent.[13−17] On longer time and length scales, the presence of phonon-type modes of the DNA backbone has been reported.[18,19] Furthermore, the finely balanced thermodynamic impacts of changes in solvation, base stacking, and interstrand pairing interactions control not only the structure but also the structural stability.[20−24]

We have demonstrated recently that ultrafast 2D-IR spectroscopy can be used as a tool to resolve the molecular interactions of DNA−ligand complexes in solution, reporting

studies of Hoechst 33258 (H33258) binding to dsDNA oligomers.[25] H33258 is a well-established minor groove binder and fluorescent dye whose derivatives show antibacterial activity as well as bacterial topoisomerase I inhibition.[26] H33258 typically binds to AT-rich sequences of DNA in a 1:1 stoichiometry and preferentially targets A-tract sequences (A_nT_n, $n \geq 2$), exhibiting nanomolar binding constants,[27,28] although binding is known to be influenced by the ratio of ligand to DNA and DNA hydration.[29−32] Changing the base sequence to an alternating $(AT)_n$ motif leads to an order of magnitude reduction in binding affinity. By comparing H33258 binding to sequences featuring A-tract and alternating motifs, it was possible to compare optimal and suboptimal ligand binding cases. 2D-IR spectroscopy revealed that optimal binding is accompanied by an additional subtle structural rearrangement of base propeller twists within the dsDNA structure that augments the altered solvation of the minor groove found in both optimal and suboptimal scenarios.[25] This was interpreted as further support for the induced-fit binding mechanism to A-tract DNA proposed following results obtained from NMR measurements on similar systems.[33]

Moving beyond our long-held perception of static bio-molecular structures to observe dynamics is technologically challenging. Temperature-jump initiation has been used to study the dynamics of nucleic acids. Examples include following the conformational dynamics of DNA with fluorescence resonance energy-transfer detection both alone and in complex with proteins.[34,35] Temperature-jump (T-jump) initiation has also been combined with ultrafast infrared spectroscopic probing to yield base-specific measurements of nucleic acid melting processes in RNA[36,37] and, more recently, in dsDNA sequences.[38,39] These experiments revealed two main dynamic timescales involved in dsDNA melting (70−100 ns and 10−30 μs) that were assigned to end-fraying and separation of the DNA duplex into single-stranded forms (DNA melting), respectively. Studies of a series of oligomers with two GC base pairs implanted into an AT sequence at the ends, in the center, and at intermediate points reported that end-fraying was observed in all but the case where the GC bases were placed at the ends of the sequence, the latter resulting in a two-stage melting mechanism.[38,39]

In this article, we employ T-jump-initiated ultrafast IR spectroscopy to extend our understanding of how H33258 binding influences DNA structure to explore the dynamic implications of molecular association.[25] By inducing a nano-second temperature jump of 9 °C to DNA−H33258 complexes featuring A-tract and alternating $(AT)_n$ binding motifs, the melting behavior of the sequences was followed on timescales from a few nanoseconds to 1 ms. Base-specific insight into the melting mechanism was achieved by the use of IR wavelength probe pulses. In the case of the A-tract sequence, the presence of the ligand led to a dramatic increase in melting timescales from 30 to ∼250 μs. Ligand binding also suppressed premelting disruption of the dsDNA structure, including end-fraying processes, which took place on 100 ns timescales. Ligand binding to alternating sequence dsDNA led to a smaller increase in melting timescales and reduced suppression of premelting sequence perturbation and end-fraying relative to the unbound DNA. These results demonstrate a dynamic impact of the minor groove ligand on the dsDNA structure that correlates with the ligand binding strength.

■ MATERIALS AND METHODS

DNA. All DNA oligomers (5′-GCAAATTTCC-3′ and 5′-GCATATATCC-3′ and their complementary sequences) were purchased as salt-free, lyophilized solids from Eurogentec. All other chemicals were purchased from Sigma-Aldrich and used without further purification. In all cases, the dsDNA concentration was 10 mM in a deuterated TRIS buffer (100 mM TRIS, 100 mM NaCl, pD 7.0). Solutions containing H33258 were prepared by annealing the dsDNA with the ligand in equimolar ratio. The high affinities shown by H33258 for these sequences mean that there is no appreciable amount of free DNA in either case.[32]

IR Absorption Spectroscopy. Measurements of dsDNA melting were performed on a Nicolet iS10 spectrometer (Thermo Fisher Scientific) at a frequency resolution of 4 cm^{-1}. The sample temperature was adjusted by a temperature-controlled liquid cell with resistive heating accurate to ±1 °C. For all infrared spectroscopy experiments, including T-jump measurements, the sample was held between two 2 mm-thick CaF$_2$ windows separated by a 6 μm-thick spacer.

T-Jump Spectroscopy. The T-jump pump, mid-IR probe spectrometer used for DNA melting experiments was located within the ULTRA Facility at the STFC Rutherford Appleton Laboratory. The method was based upon the ime-resolved multiple-probe spectroscopy (TRMPS) strategy demonstrated previously for photochemical activation.[40,41] T-jump excitation pulses were produced at a repetition rate of 1 kHz using a homebuilt Nd:YAG-pumped optical parametric oscillator (OPO). The ∼4 ns duration pulses produced had a maximum energy of 70 μJ at 2660 cm^{-1}, resonant with the high-frequency wing of the OD stretching vibration of D$_2$O, allowing sample heating while avoiding complete absorption of the pump radiation by the solvent. At a path length of 6 μm, the sample absorbance was 1.6, and measurements of the pump energy immediately before and after the sample indicated a reduction in the pulse energy from 70 to 18 μJ. The T-jump pulse train was optically chopped to give a repetition rate of 0.5 kHz. Mid-IR probe pulses were generated by an amplified Ti:sapphire laser system pumping an optical parametric amplifier equipped with difference frequency mixing of the signal and idler outputs. The pulse duration and center frequency of the mid-IR pulses were 50 fs and 1630 cm^{-1}, respectively; the latter was coincident with the characteristic base vibrational modes of dsDNA. The difference between the 10 kHz repetition rate of the Ti:sapphire laser and the 0.5 kHz repetition rate of the T-jump pump pulses, combined with the use of an electronic delay to control the relative pulse timings of the pump and probe laser systems, enabled collection of T-jump pump IR probe spectra at time delays (τ_{pp}) from 1 ns to 2 ms. Calibration of the T-jump spectrometer with trifluoroacetic acid solutions established that the T-jump obtained was 9 °C and that cooling of the sample was completed by 1 ms. Experimental details are provided in the Supporting Information (Figures S1−S4) and will be the topic of a forthcoming publication.

Data Management and Preprocessing. The T-jump IR probe spectroscopy data were obtained using a reference detector to reduce the impact of pulse-to-pulse energy fluctuations of the probe laser. Reproducible signals from the thermal response of the buffer solution and an electronic response from the triggering of the nanosecond pulse generation system were also subtracted routinely from the data (see Figure S5 for details).
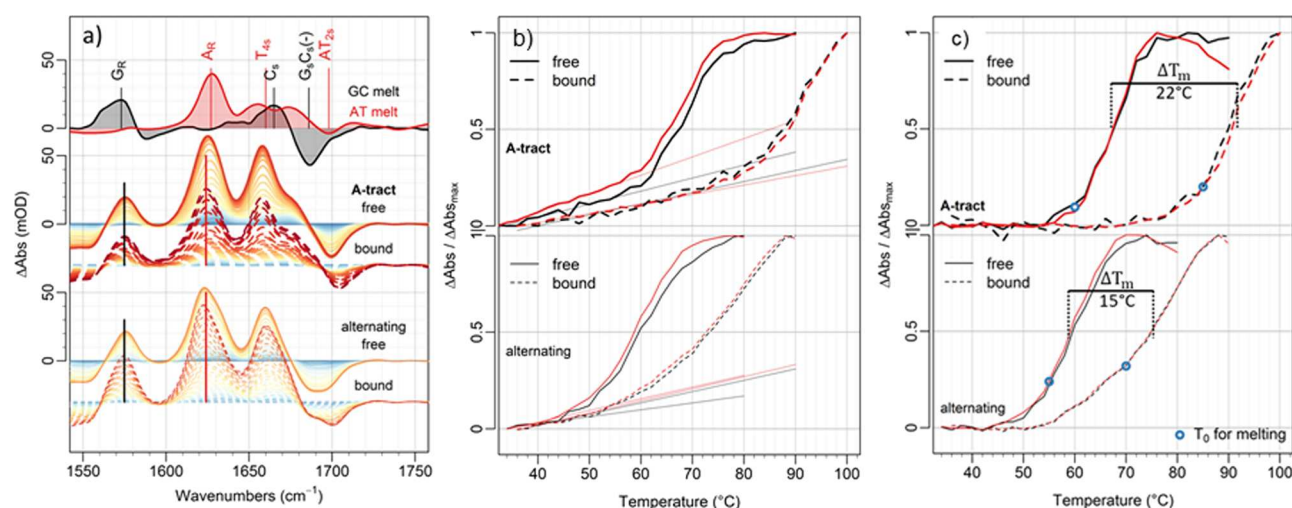
Figure 1. (a) Top: IR absorption difference spectra showing the impact of melting on the IR spectrum of dsDNA sequences containing only GC (GC melt, black) and AT (AT melt, red) base pairs. Assignments for significant bands based on a previous work are given in the figure.[25] Middle: IR absorption difference spectra for the free A-tract dsDNA sequence (solid lines) as a function of temperature. Corresponding data for the bound A-tract sequence are shown as dashed lines. The spectra are vertically offset for clarity, and scale bars are given to the left of the figure. The temperature scale runs from 30°C (blue) to 90 (red) °C in 2 °C steps. Bottom: IR absorption difference spectra for the free alternating dsDNA sequence (solid lines) as a function of temperature. Corresponding data for the bound alternating sequence are shown as dashed lines. (b) Melting curves for the A-tract (top) and alternating (bottom) dsDNA sequences under free (solid) and bound (dashed) conditions. The black traces show the normalized intensity of the G_R mode shown in (a), and the red traces show corresponding results for the A_R mode. (c) As (b) but a sloping premelting response has been subtracted by first fitting to a straight line in all cases (see b) to isolate the sigmoidal response. Blue circles show the starting temperature (T_0) for T-jump melting experiments, the results of which are shown in Figure 2.

RESULTS

IR Absorption Spectroscopy. IR absorption spectra were obtained at a range of temperatures for dsDNA oligomers containing a central A-tract (5′-GCAAATTTCC-3′ and complementary sequence) and an alternating arrangement of AT base pairs (5′-GCATATATCC-3′ and complementary sequence), both in the presence (bound) and absence (free) of H33258. It has been established previously that H33258 binds strongly to the central AT-rich region of both sequences.[25]

The results of IR absorption spectroscopy experiments carried out on the free dsDNA sequences (Figure 1a solid lines) are presented as difference spectra relative to the absorption spectrum of the sequences at 30 °C before melting begins. The color progression from blue to red indicates the impact of increasing the temperature of the sample from 30 to 80 °C in steps of 2 °C for the alternating sequence. For the A-tract sequence, a final temperature of 90 °C was used, reflecting the slightly higher melting temperature of the A-tract dsDNA.[25] The spectra prior to subtraction are shown in Figure S6. For both the A-tract and alternating sequences, bands in the IR absorption spectrum located at 1660, 1622, and 1575 cm^{-1} were observed to increase in intensity as the temperature increased (blue to red in Figure 1a), while a band at 1700 cm^{-1} decreased in intensity. These results are consistent with previous studies of mixed GC/AT sequence dsDNA melting using IR absorption and 2D-IR spectroscopy.[25,38,39,42−46] The top row of Figure 1a shows difference IR absorption spectra obtained upon melting of dsDNA sequences featuring only GC (black) or AT (red) base pairs[42] along with band assignments based on prior work.[25,38,39,42] These show that the 1575 cm^{-1} band can be assigned to a G ring stretching vibrational mode (G_R), and the 1622 cm^{-1} mode is attributable to an A ring vibrational mode (A_R), while the 1700 cm^{-1} mode is due to the T_2 carbonyl stretching vibration. The peak at 1660 cm^{-1} is a mixture of GC- and AT-derived vibrational modes.

For the purposes of time-resolved studies of strand melting, the G_R and A_R modes are well separated from overlapping contributions and both increase significantly in intensity upon dsDNA melting. These modes thus act as base-specific markers for GC and AT melting dynamics, respectively, and we will focus upon these bands from here on. Plotting the normalized intensity change of these two modes for the free A-tract and alternating sequences as a function of temperature (Figure 1b,c, solid lines) shows that both the G_R (black) and A_R (red) modes increase in intensity following identical sigmoidal profiles for each sequence, reaching midpoints at 68 °C for the A-tract and 60 °C for the alternating sequences. This behavior is consistent with the duplex melting, and the midpoint temperatures (T_m) are consistent with previous studies of these sequences, which showed small departures from simple two-state fitting models.[25]

The impact of H33258 binding on the form of the temperature-dependent IR absorption spectra of the A-tract and alternating sequences is minor (Figure 1a, dashed lines). H33258 does not feature strong IR absorptions in the DNA base stretching mode region of the spectrum, and ligand binding causes no suppression of the signal intensities at a given temperature.[25] In the case of the bound sequences, the marker G_R and A_R modes both increased in intensity as the temperature was raised. Indeed, the total change in absorbance for the two bands was very similar to that observed for the free sequences. The presence of the ligand does, however, shift the T_m value of the A-tract and alternating sequences upward by 22 and 15 °C, respectively (Figure 1c, dashed lines). The sigmoidal melting curve shows a slightly reduced gradient in the case of the bound alternating sequence. The observed increase in strand melting temperature (ΔT_m) upon H33258 binding to the A-tract sequence is indicative of strong ligand-induced thermodynamic stabilization of the dsDNA. The effect is somewhat reduced in the alternating sequence, consistent with an order of magnitude reduction in binding affinity for the alternating sequence
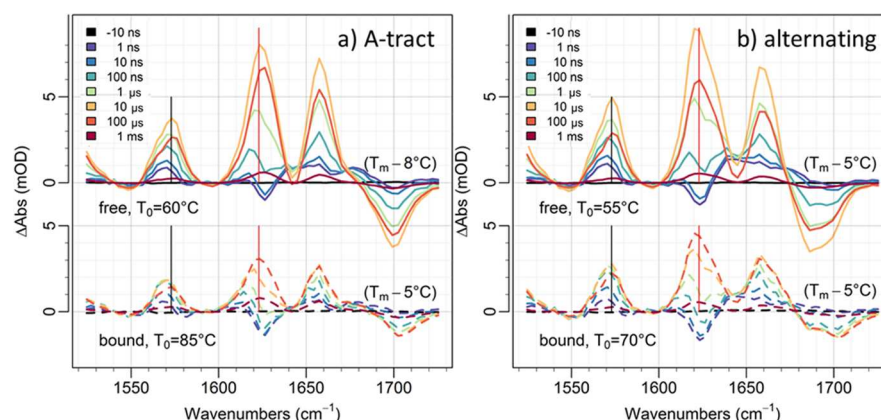
Figure 2. Temperature-jump IR spectroscopy results for (a) A-tract and (b) alternating sequence DNA under free (top, solid lines) and bound (bottom, dashed lines) conditions. The data shows difference spectra (T-jump pump on−pump off) as a function of T-jump pump IR probe delay time (τ_{pp}) as per the legend. The T_0 value for each dataset relative to T_m for the sequence is shown in the figure. Black and red vertical lines indicate the G_R and A_R marker modes, respectively.
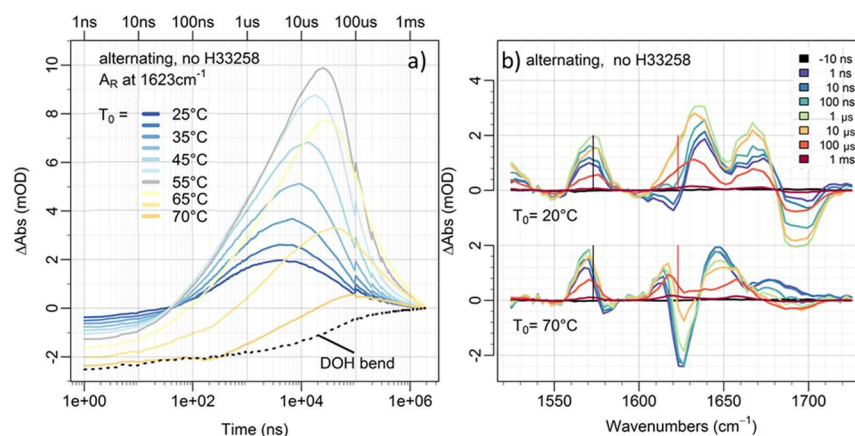

Figure 3. (a) Time traces of the magnitude of the A_R mode of the free alternating dsDNA sequence as a function of T_0. As the T_0 value increases toward T_m for the sequence (60 °C), the maximum amplitude of the response increases as would be expected for a signal derived from dsDNA strand melting. The response of the buffer solution is shown as a black dashed line. (b) T-jump IR spectra of the free alternating dsDNA sequence obtained at T_0 values of 20 °C (top) and 70 °C (bottom).

compared to the A-tract.[25] No significant difference in the melting profiles of the A_R and G_R modes, and by implication the AT and GC base pairs, was observed for either the free or bound sequences.

Temperature-Jump IR Spectroscopy. The results of representative T-jump spectroscopy measurements are shown in Figure 2a for the free (upper, solid) and bound (lower, dashed) A-tract sequence. The color progression extends from τ_{pp} values of 1 ns (violet) to 1 ms (red). The spectra in Figure 2a are difference spectra obtained by subtracting the IR probe pulse profile in the absence of the T-jump pulse from that when the T-jump pulse was present for a starting temperature (T_0) of 5 °C below the measured T_m for the sequence. The spectral profiles should thus be directly comparable to the IR absorption difference spectra shown in Figure 1a. The data for the free A-tract sequence shows that the sample responds instantaneously on the timescale of the nanosecond duration T-jump pulse. The purple (τ_{pp} = 1 ns) spectrum contains positive peaks at 1580, 1650, and 1670 cm^{-1}, indicating that these peaks gain in intensity in the presence of the T-jump pulse. In addition, negative peaks appear at 1630 and 1700 cm^{-1}, showing the presence of peaks that decrease in intensity following the T-jump. The peak at 1580 cm^{-1} shifts slightly to higher

wavenumber over the first 10 ns, while the 1630 cm^{-1} peak shifts to lower wavenumber and becomes positive in sign; thereafter, all peaks increase in magnitude, reaching maxima at around τ_{pp} = 10 μs (orange spectrum), before decaying to the baseline. The T-jump spectra of the free alternating sequence show nearly identical spectral features to those observed for the free A-tract sequence (Figure 2b, solid lines).

Figure 3a shows typical T-jump time traces for the amplitude of the A_R band at 1622 cm^{-1}. The figure shows results for the free alternating sequence, but comparable results were obtained for both sequences studied. Four distinct response regimes are visible in the T-jump time traces (Figure 3a). An instantaneous, subnanosecond response is followed by a small increase in intensity of the A_R peak on 100 ns timescales. A larger increase in intensity occurs on tens of microsecond timescales, before the signal returns to the baseline by 1 ms. We note that the response of the buffer has been subtracted from all of the DNA datasets presented.

The spectral features present at τ_{pp} = 10 μs (Figure 2) exactly match the peaks in the IR absorption difference spectra (Figure 1) assigned to strand melting, suggesting that this process is occurring in the T-jump experiment. Further support for this assignment arises from the fact that the maximum amplitude of
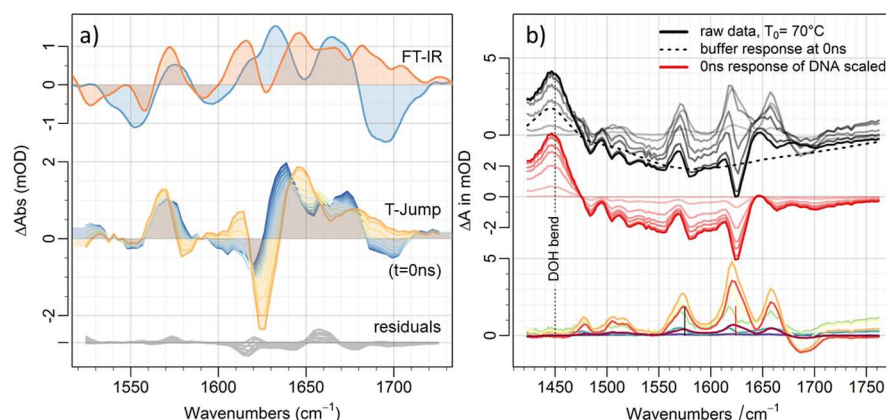
Figure 4. (a) Top: IR absorption difference spectra of free A-tract dsDNA following a 4 °C temperature rise beginning from 32 °C (blue) and 86 °C (orange). Middle: T-jump pump IR probe spectra of free A-tract dsDNA obtained with a T-jump probe delay time (τ_{pp}) of 0 ns as a function of T_0 from 20 °C (blue) to 70 °C (orange). Bottom, residuals obtained following fitting of T-jump pump IR probe spectra of free A-tract dsDNA obtained with τ_{pp} = 0 ns to a linear combination of the T_0 = 20 and 70 °C responses (see text). (b) Effect of subtracting combined effects of the instantaneous dsDNA thermal response and the buffer response from T-jump IR spectra. Black/gray traces show raw T-jump IR spectra for a T_0 of 70 °C. The buffer response is shown as a dashed line. Red/pink traces show the linear combination of the dsDNA τ_{pp} = 0 ns response and the buffer solution. Lower traces show the result of subtracting the τ_{pp} = 0 ns dsDNA/buffer combination from the raw T-jump IR spectroscopy data where the signals due to dsDNA melting are clearly isolated. In the lower trace, the color scheme indicates τ_{pp} identically to Figures 2 and 3.

the A_R peak in the T-jump data increased with increasing T_0 (Figure 3a, blue to orange), reaching a peak at T_0 = 55 °C. The latter is 5 °C below the T_m for the free alternating sequence as would be expected, given the calibrated T-jump magnitude of 9 °C and the sensitivity of the A_R band intensity to strand separation (Figure 1).

Examining the spectral response of the free dsDNA sequences at shorter τ_{pp} values (Figure 2a, blue and green spectra) shows that the spectral pattern present at the 10 μs signal maximum appears between 10−100 ns, suggesting that processes giving rise to the same spectral features as strand separation are already occurring on these shorter timescales. This is consistent with observations of disruption of the dsDNA structure on submicrosecond timescales, reported previously as end-fraying.[38,39] The progressive change in the value of τ_{pp} at which the peak signal is observed with T_0 in Figure 3a is related to the balance of these faster processes and melting dynamics, and we give a detailed discussion of these dynamics below. The decrease in the A_R signal on millisecond timescales is attributed to the sample cooling and reforming of the dsDNA.

Comparing the results of T-jump experiments on bound sequences to those of the free dsDNA (Figure 2a,b, dashed lines) shows that the same spectral profiles were observed for both sequences when the ligand was present. It is notable that the magnitude of the observed features was somewhat smaller than that observed for the free sequences, although relative intensity ratios of the bands were maintained, indicating that the same processes are being observed for the dsDNA−ligand complexes as for the free dsDNA. Prior to carrying out a complete analysis of these T-jump melting dynamics, however, it is necessary to consider the presence and temporal behavior of the instantaneous (subnanosecond) response of the dsDNA to the T-jump pulse in more detail.

Subnanosecond Response. An instantaneous response to the T-jump pulse was observed for all samples studied. This is indicative of fast dynamic processes that are not temporally resolved as a result of the nanosecond duration of the T-jump laser. The shift in peak positions occurring over the first 10−100 ns in the T-jump spectra for all sequences (Figure 2)

demonstrates that the molecular origin of this instantaneous effect differs from the dynamics observed from 10 ns onward.

To understand the subnanosecond response in more detail, Figure 3b shows spectral data from T-jump measurements of the free alternating sequence obtained at T_0 values both well below (T_0 = 20 °C, upper trace) and above (70 °C, lower) the dsDNA melting transition. It is clear that, even when starting well below the T_m value of the sequence, $(T_0 - T_m)$ = −40 °C, the subnanosecond response is present, and its spectral form is similar to the subnanosecond response observed with $(T_0 - T_m)$ = −8 °C (Figure 2b). In contrast to Figure 2, however, the data in Figure 3b shows that, when T_0 is further away from T_m, there is relatively little evolution in either amplitude or peak position as the subnanosecond spectral response decays to the baseline within 1 ms. This is as would be expected if no strand melting occurs in the experiment.

At a T_0 of 70 °C, where $(T_0 - T_m)$ = +10 °C and a mixture of ds and ssDNA is expected (Figure 3b (lower)), the initial response of the sample is different to that observed at T_0 = 20 °C, showing that the subnanosecond response is influenced by the dsDNA:ssDNA concentration ratio. In this case, the T-Jump signal evolves from τ_{pp} = 0 ns (purple spectrum) to yield a new set of bands at 100 μs (red spectrum) that includes a small rise of the G_R and A_R marker modes (black and red vertical lines), indicative of a component of melting. Once again, this is as would be expected because, just above the T_m, a fraction of dsDNA remains in the sample.

These sample-dependent subnanosecond spectral features persist for too long to be consistent with a pulse cross-correlation effect (Figure 3b), ruling out a purely instrumental response. We thus ascribe the observed subnanosecond signals to shifts in DNA vibrational modes caused by changes in DNA solvation and H-bonding in response to the elevated temperature and concomitant reduced density of the solution.

To demonstrate that this is a reasonable assignment, we compare the subnanosecond T-Jump response of free A-tract DNA (Figure 4a, center) as a function of T_0 (blue-orange) with difference IR absorption spectra (Figure 4a, top) obtained following 4 °C temperature changes beginning from 32 °C (Figure 4a, blue) and 86 °C (Figure 4a, orange). These
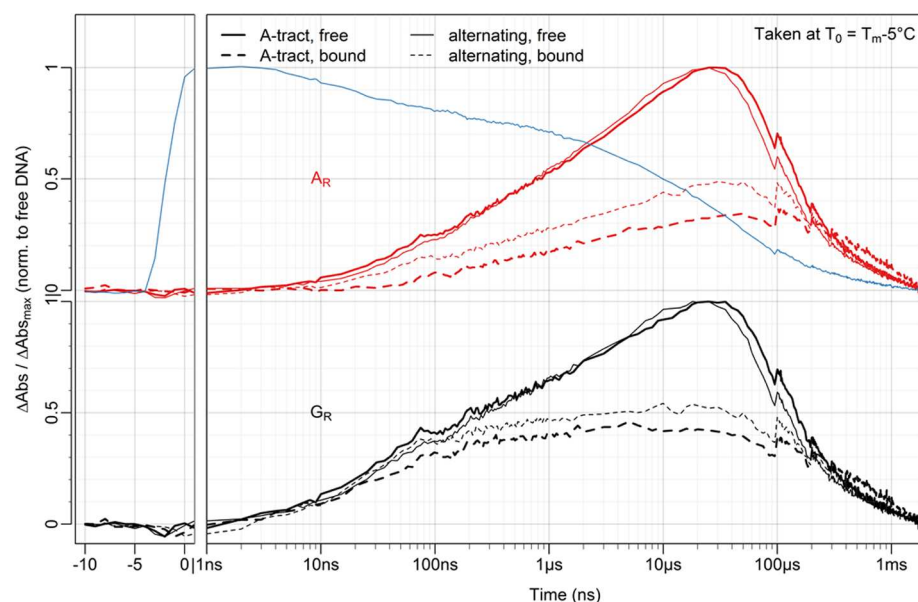
Figure 5. Time traces of the magnitude of the A_R (red, 1622 cm^{-1}) and G_R (black, 1575 cm^{-1}) marker bands obtained from T-jump IR experiments. Results are shown for the A-tract (bold line) and alternating (light line) sequences under free (solid) and bound (dashed) conditions. The temporal response of the buffer solution at the wavenumber of both the A_R and G_R transitions is shown in blue.

parameters were chosen to reflect a small increase in T beginning well below and above T_m, respectively. The subnanosecond T-Jump responses at low (blue) and high (orange) starting temperatures show a strong similarity to the IR absorption difference spectra. Furthermore, all of the subnanosecond T-jump responses at T_0 values intermediate between 20 and 70 °C could be accurately reproduced by a linear combination of the T_0 = 20 °C and T_0 = 70 °C traces. The residuals from this fitting process are shown as gray traces in Figure 4a. Thus, the instantaneous response of any given sample to a temperature-jump could be derived from a linear combination of the instantaneous temperature responses of the ss and dsDNA present in the sample.

Examining the temporal evolution of the subnanosecond response in the absence of significant amounts of dsDNA melting shows that the dynamics follow the response of the buffer. This can be seen by the similarity of the dashed black trace in Figure 3a, which shows the response of the HOD band at 1450 cm^{-1} to the orange trace and the response of the free alternating sequence at T_m = 70 °C, well above T_m. This adds further weight to the assignment of the subnanosecond process to a thermal response of the dsDNA without melting occurring.

In addition to assigning a portion of the T-jump response, thorough characterization of the instantaneous response of the dsDNA allows a more sophisticated separation of the initial thermal response of the sample from the later melting dynamics. By combining the temporal response of the buffer at 1450 cm^{-1} (Figure 3a) with the T-jump spectral response of the DNA sample at τ_{pp} = 0 ns and subtracting these features from the raw T-jump data, it was possible to isolate the melting dynamics of the dsDNA more cleanly. Figure 4b shows the results of this approach. The raw T-jump IR spectral data includes the thermal response of the DNA obtained with a T_0 of 70 °C (black/gray) and the response of the HOD bending vibrational mode of the buffer solution at 1450 cm^{-1}. The subnanosecond spectrum of the buffer solution alone is shown as a black dashed line. The calculated subnanosecond responses of the DNA based on the concentrations of ss and dsDNA expected at this T_0 value were

combined with the measured buffer response as a function of τ_{pp} (red/pink traces). The lower traces show the results of subtracting this combined thermal background from the T-jump data. The subnanosecond response is removed, and the remaining peaks show only dynamics consistent with dsDNA melting. All data presented henceforth have undergone this procedure.

DNA Melting Behavior. Using the A_R and G_R responses as base-specific marker modes allows examination of the melting dynamics of dsDNA. The dynamics of the two bands are shown in Figure 5, which compares the A_R mode (red) with the G_R mode (black) for the A-tract (bold line) and alternating (lighter line) sequences under free (solid) and bound (dashed) conditions. The data were obtained with $(T_0 - T_m)$ values of −5 °C, corresponding to the spectral data shown in Figure 2. The time traces have been normalized to the maximum A_R or G_R signal for the free sequences, but the ratio of the signal amplitudes between free and bound sequences has been conserved. The reason for this is to reflect the lower intensities of the peaks obtained for the bound sequences compared to the free sequences (cf. solid and dashed spectra in Figure 2a,b). The blue line shows the temperature profile of the T-jump for reference.

Qualitatively, it can be seen (Figure 5) that the AT and GC base pairs of the free sequences melt on similar timescales, with the peak in the A_R (red) and G_R (black) responses both occurring near 30 μs. This is the case for both the A-tract (bold) and alternating (light) sequences. Additionally, both the GC base pairs at the ends of the sequences and the AT base pairs in the center demonstrate a rising signal on 100 ns timescales. This is more apparent in the GC case (Figure 5, black) than the AT (red) case, but the results of data fitting, presented below, show that it is observed in both.

Binding of the H33258 ligand has three significant impacts on the melting of the dsDNA. First, the peak melting signal is shifted to later values of τ_{pp}, but the A_R and G_R responses are still simultaneous. Second, the maximum amplitudes of the A_R and G_R responses are reduced by at least 50% for all ligand/DNA

combinations. Given that neither a corresponding decrease in the IR absorption difference spectral amplitudes (Figure 1) nor a significant reduction in the temperature-gradient of the melting transition upon H33258 binding that could account for this was observed, this is suggestive of delayed melting dynamics leading to the DNA melting signal being suppressed. This suppression occurs because the melting process is taking place on similar timescales to the sample cooling (Figure 5, blue trace). Support for this can be obtained from the results for the free A-tract DNA sequence. Equilibrium IR absorption data suggests a maximum expected change in signal upon melting of 12−14 mOD, whereas the observed signal is around 8 mOD (Figure 2). This suggests a small amount of signal reduction caused by sample cooling and would be consistent with previous studies that showed a peak in the melting curve occurring at slightly later times.[38,39]

Finally, the faster (100 ns) response of the GC base pairs appears to be largely conserved upon H33258 binding whereas that of the AT base pairs is suppressed in amplitude. This can be seen by the fact that there is relatively a little change in the G_R mode response over the first 100 ns upon ligand binding (cf. solid and dashed black lines, Figure 5).

To quantify the dynamics observed, the temporal behavior of the A_R and G_R marker bands was fit to a sum of two stretched exponential functions. The data was first normalized to the solvent response to account for the effects of the cooling solvent on the signal amplitudes, and the fitting was carried out in the range from 0 ns to 40 μs

$$\Delta A(t) = -\alpha_1 e^{\left(-\frac{t}{\tau_1}\right)^{\beta_1}} - \alpha_2 e^{\left(-\frac{t}{\tau_2}\right)^{\beta_2}} + \alpha_1 + \alpha_2 \quad (1)$$

The results are shown in Figure 6 and Table 1. Due to the normalization, amplitudes α_1 and α_2 will sum to unity for traces from free DNA samples. It was necessary to include a stretching exponent (β_1, β_2) for both exponential terms to obtain a converging fit. The β values obtained range from 0.5 to 1 (Table 1), indicating that the observed kinetics arise from a slightly heterogeneous ensemble that cluster around τ_1 and τ_2. The need for β_1 and β_2 to accurately model the dynamics may arise from nonuniform heating across the sample. The strong absorption of the pump pulse (Figure S4) means that the initial temperatures at the front and back face of the sample will differ. Based on the measured ΔT of 9 °C, we estimate this to be ±3 °C at τ_{pp} = 0 ns, but this distribution narrows as τ_{pp} increases.[47] Other possible origins of the stretching of the exponential may arise from the fact that each G_R and A_R peak contains contributions from a number of base pairs and previous observations of rugged energy landscapes with small energy barriers, which we return to below.[34−36]

The fitting results (Table 1) confirm the qualitative observations that melting of free DNA sequences proceeds on two timescales, one submicrosecond (τ_1) and the other in the range 10−30 μs (τ_2). The main melting process is assigned to τ_2 where it can be seen that both the A_R and G_R marker modes display near identical dynamics, suggesting concerted melting. Although the normalization of the data to the buffer response necessarily assumes a linear response of the signal amplitude to the changing temperature in the sample, which is a potential source of error, these results are in excellent agreement with recent studies of DNA melting in similar DNA sequences with a slightly different GC/AT composition.[38,39] The timescales observed in our experiments also agree well with those observed in T-jump studies of RNA-based sequences, although in those experiments, a third, slower set of dynamics on hundreds of microseconds timescales was also reported.[37]

The faster τ_1 dynamics were observed in our measurements for both the GC base pairs at the ends of the sequence and the AT base pairs in the center, although it is noticeable that the timescale of these processes is shorter for the terminal GC base pairs (∼100 ns) than the central AT component (∼600 ns). These trends are reproduced for the alternating sequence, although the AT timescale is shorter (∼250 ns).

These faster processes have previously been assigned to end-fraying and this is not inconsistent with their more dominant presence in the GC base pairs as observed here.[38,39] It was reported that these signals were very small for sequences with GC ends and AT cores, and the greater GC component in the sequences studied here will contribute to a larger signal from these bases. The fact that these fast processes are observed in the AT core in our data shows that a perturbation of the equilibrium structure of the bases is occurring along the full length of the oligomer. It is entirely plausible that some of this perturbation is due to end-fraying, but our data are not consistent with this being the sole cause. The large amplitude change in A_R marker modes upon dsDNA melting is widely ascribed to the loss of base stacking rather than the Watson−Crick H-bond dissociation.[48] This supports the assignment of these fast dynamics (τ_1) to strand perturbation affecting base stacking, and microsecond timescale dynamics of RNA sequences have been ascribed to base stacking-related processes;[36] however, end-fraying will necessarily impact upon base stacking, and so it is impossible to fully differentiate the two processes based on this vibrational mode. It is noteworthy that previous reports employed a dispersed vibrational echo probe signal rather than the absorption approach that we employ here.[38,39] The former is more sensitive to the effects of base pairing via Watson−Crick-induced vibrational coupling, although a component of the signal will still reflect changes in base stacking. The shorter τ_1 timescales of the AT central section in the alternating sequences
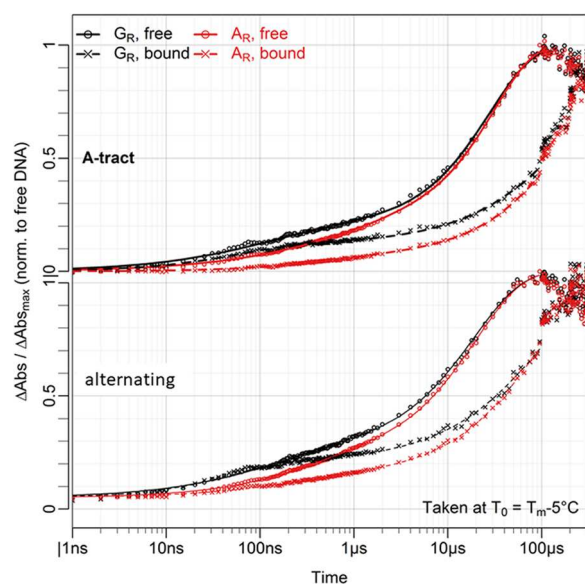

Figure 6. Time traces of the magnitude of the A_R (red) and G_R (black) marker bands obtained from T-jump IR experiments normalized to the solvent response. Results are shown for the A-tract (upper) and alternating (lower) sequences under free (circles) and bound (crosses) conditions.

Table 1. Parameters Obtained Following Bi-exponential Fitting of T-Jump Data

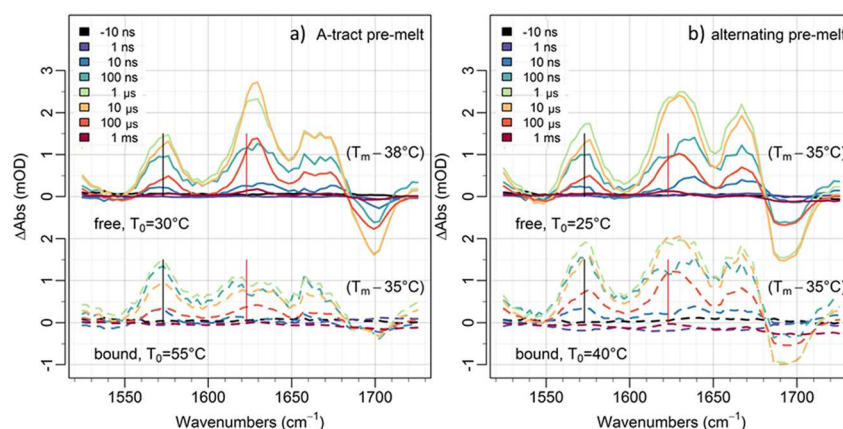|	α_1		α_2		τ_1 in ns		τ_2 in μs		β_1		β_2	
sequence	G	A	G	A	G	A	G	A	G	A	G	A
free A-tract	0.20	0.24	0.80	0.76	110	700	28	32	0.6	0.5	0.9	1.1
bound A-tract	0.12	0.06	0.88	0.94	60	530	280	240	0.7	0.7	0.7	0.8
free alternating	0.21	0.18	0.79	0.82	130	280	19	20	0.6	0.7	0.9	0.9
bound alternating	0.16	0.09	0.84	0.91	50	210	110	96	0.8	0.6	0.7	0.8

Figure 7. Premelting temperature-jump IR spectroscopy results for (a) A-tract and (b) alternating sequence DNA under free (top, solid lines) and bound (bottom, dashed lines) conditions. The data shows difference spectra (T-jump pump on−pump off) as a function of τ_{pp} as per the legend. The T_0 value for each dataset is shown in the figure. Black and red vertical lines indicate the G_R and A_R marker modes.

as compared to the A-tract sequence observed in our data indicate a more dynamic core in the alternating sequence. These observations apparently correlate with the lower melting temperature of this sequence and with sequence-dependent stacking energies.[49]

Binding the H33258 ligand to the A-tract sequence (Table 1) has a relatively little effect on the shorter (τ_1) timescales, the rates of which get slightly faster for both the G_R and A_R modes (60 vs 100 ns and 530 vs 700 ns, respectively). However, the relative amplitude of these processes is reduced in both cases. This reduction is significant in the case of the central AT sections, which constitute the binding region ($\alpha_{1,bound}/\alpha_{1,free} = 25\%$), but suppression is also observed for the GC base pairs ($\alpha_{1,bound}/\alpha_{1,free} = 60\%$), which are located outside of the ligand binding region. The longer timescale (τ_2) melting is still a concerted process involving both AT and GC base pairs together, but the overall timescale is nearly an order of magnitude longer ($\sim 250\ \mu$s), indicative of very strong stabilization of the duplex structure. Given that the cooling sample effectively precludes observation of timescales beyond $100\ \mu$s, this numerical value must be taken as indicative only, but the significant slowing down of melting dynamics is clear. It is notable that this stabilization also extends beyond the binding region, affecting the GC units as well as the central AT section of the sequence.

In the case of the alternating sequence, similar results were obtained to those of the A-tract sequence, although, crucially, the impact of H33258 on the dynamics is less dramatic. The suppression of the amplitudes of the faster (τ_1) processes is less significant ($\alpha_{1,bound}/\alpha_{1,free} = 50\%$ for A_R; 76% for G_R) than that observed for the A-tract sequence. The impact of ligand binding upon the melting dynamics is also less emphatic, with an increase by a factor of 5 in the melting timescale ($110\ \mu$s).

DNA Premelting Response. The dynamics observed following T-jump experiments with T_0 values well below T_m

are informative in understanding the impact of H33258 binding upon dsDNA. Figure 7 shows spectra for the A-tract (Figure 7a) and alternating (Figure 7b) sequences under free (solid lines) and bound (dashed) conditions at $(T_m - T_0) = -35\ °C$. With a T-Jump of 9 °C, the majority of the DNA should remain in the ds configuration throughout this experiment.

The spectral features of the free DNA sequences (Figure 7a,b; top, solid lines) at τ_{pp} values of $10\ \mu$s are in good agreement with responses shown in Figure 2, albeit with a much smaller overall change in absorbance (~ 2 mOD peak amplitude vs ~ 10 mOD) as a result of the reduced levels of strand melting. It is however interesting to note that, for the bound sequences, the relative intensity ratios of the peaks do not remain constant as they did for experiments carried out with T_0 closer to T_m. Specifically, while the G_R modes in the bound sequences rise to the same amplitude as in the free sequences, the A_R modes are relatively smaller. This further indicates that the AT base pairs in the binding region are more stable than the GC base pairs at the ends of the sequences and confirms that, below the melting transition, AT base pairs are stabilized by the ligand and show a smaller response in the T-Jump experiment. By contrast, the GC base pairs show less suppression of strand perturbation and end-fraying. This result is apparent in the alternating sequence as well as the A-tract (Figure 7b).

The temporal traces of the A_R (red) and G_R (black) modes in these pre-melting experiments are shown in Figure 8 (traces not normalized). As expected, these traces lack the large rise in intensity on microseconds timescales that has been assigned to strand melting. Instead, only a small rise on nanosecond timescales is observed, consistent with strand perturbation and end-fraying. Each trace was fitted from 0 to $100\ \mu$s to the sum of an exponential rise and a decay
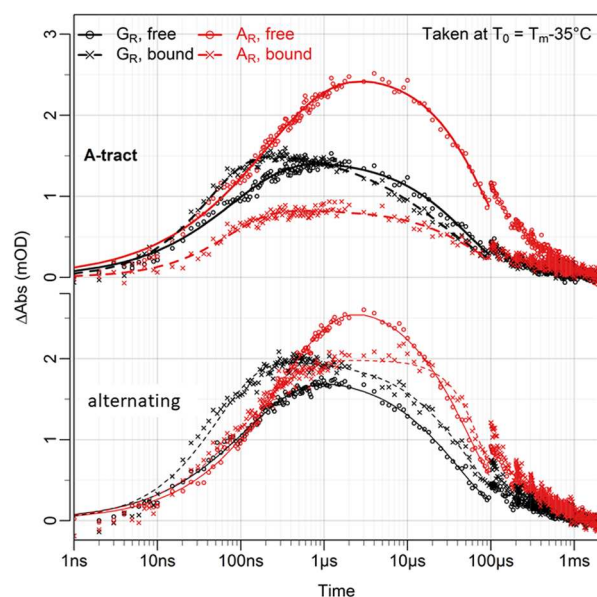
Figure 8. Time traces of the magnitude of the A_R (red) and G_R (black) marker bands obtained from premelting T-jump IR experiments (Figure 7). Results are shown for the A-tract (upper) and alternating (lower) sequences under free (circles) and bound (crosses) conditions.

$$\Delta A(t) = \alpha \left(-e^{\left(-\frac{t}{\tau_{\text{rise}}}\right)^{\beta_{\text{rise}}}} + e^{\left(-\frac{t}{\tau_{\text{decay}}}\right)^{\beta_{\text{decay}}}} \right)$$

(2)

where α denotes the total peak amplitude. The results of the fits are summarized in Table 2. Rise times of 40−120 ns (G_R) and 70−300 ns (A_R) are consistent with results where melting behavior was studied (Table 2), but low peak amplitudes of a few mOD indicate that the T-Jump pulse under premelting conditions is only destabilizing the double helix, without inducing significant melting.

The data in Table 2 show that the peak amplitudes for G_R modes remain almost constant upon H33258 binding (from 1.5 to 1.6 mOD and 1.8 to 2.0 mOD for A-tract and alternating sequences, respectively), while the A_R modes again drop in intensity (from 2.5 to 0.8 mOD and 2.8 to 2.0 mOD for A-tract and alternating sequences, respectively). This is clearly visible for the A-tract sequence in Figure 8 (red traces). The suppression of the amplitude of this dynamic signal by ligand binding is again more distinctive for the A-tract sequence rather than the alternating one, signifying a quantitative difference between an A-tract and an alternating minor groove under premelting conditions. Also consistent with the melting experiments above is the decrease in timescale of the nanosecond timescale dynamics upon binding for both GC and AT base pairs. The reason for this is unclear and could relate to the higher temperatures of experiments on the bound sequences, but it could also be related to the impact of binding in the center of the strand, given that the effect is reduced when binding is less strong in the alternating sequence.

■ DISCUSSION

The principle of thermal stabilization of the DNA duplex by ligands is well known, but the molecular origins of the effect and the manner in which the ligand influences the DNA have not been fully revealed. The implication of these new results is that the presence of the ligand in the central binding section of the A-tract and alternating sequences has two major impacts:

1) The ligand reduces the degree of fast dynamic processes, such as disruption of base stacking and end-fraying, which occur on 100 ns timescales, orders of magnitude faster than full melting. These dynamics were detected across both AT and GC base pairs and were suppressed to a greater degree in the binding site than at the extremities of the sequence. The fact that an impact upon the GC base pairs was observed shows that the ligand in the minor groove leads to stabilization of base pairs located at least a few base pairs away from the ligand itself. In the current experiment, it was not possible to determine the full extent of this remote effect other than to say that it reached as far as the ends of the short sequences studied, giving a lower limit for the effect of two to three base pairs away from the binding site. The potential for such dynamic modulation by a ligand remote from the binding interaction may be the roots of allosteric binding processes on DNA strands. It is known that DNA dynamics cross a wide-range of timescales, including long-range phonon-type modes.[18] While the specific timescales measured in this experiment are longer than the THz phonon vibrations observed, the need to create a dynamic picture of DNA encompassing all relevant timescales is clearly essential to a unified view of the molecule and its interactions.

2) The ligand delays the full melting process of the DNA. This process affects all base pairs equally, with melting dynamics being retarded from 30 μs in free A-tract DNA to ~250 μs in the bound sequence. This is potentially an experimental validation of a mechanism proposed following computational simulations, which predicted that the impact of covalently bound minor groove ligands was to cause rehybridization of the strand following end-fraying, effectively reversing the nascent melting process.[9] This led to stabilization of the full strand melting dynamics. While we do not observe direct evidence for the re-forming process, the lower amplitude of the end-fraying and perturbative dynamics along with the slower melting behavior in the presence of H33258 are not inconsistent with such a scenario. This suggests that, although noncovalently bound, the H33258 ligand interacts strongly enough with the duplex DNA to substantially modify its potential energy surface.

Table 2. Parameters from Bi-exponential Fitting to Premelting T-Jump Experiments

	α in mOD		τ_{rise} in ns		τ_{decay} in μs		β_{rise}		β_{decay}	
sequence	G	A	G	A	G	A	G	A	G	A
free A-tract	1.5	2.5	80	206	52	90	0.7	0.6	0.8	1.0
bound A-tract	1.6	0.8	42	73	31	71	0.9	0.9	0.6	0.9
free alternating	1.8	2.8	118	317	41	56	0.7	0.7	0.8	0.9
bound alternating	2.0	2.0	54	126	57	89	0.9	0.7	0.8	1.7

The indication that the observed changes in the melting dynamics of DNA correlate with the binding strength of the ligand is demonstrated by the comparison of optimal (A-tract) and suboptimal (alternating) ligand binding scenarios. Such comparisons are essential to understand the molecular determinants not only for binding but also for ideal ligand binding conditions. It is clear from the T-jump measurements that, when H33258 interacts with the alternating AT binding region, the same effects observed for H33258 binding to the A-tract core are present but diluted. The slowdown observed for melting of the dsDNA is reduced in the alternating sequence, while the level of suppression of the ns fluctuations including end-fraying are also less dramatic. This suggests that the ligand has an effect on the alternating DNA sequence as would be expected for a relatively strong binding interaction; however, this effect is reduced relative to the optimized binding scenario.

It is interesting to note the consistency of the effects observed between the A-tract and alternating DNA sequences. Not only are ns fluctuations and end-fraying reduced, but the observed speed of these processes increases moderately. This suggests that, while suppressing the extent of these fluctuations, the ligand also increases their rate. This provokes a model similar to squeezing a tube in the center, simultaneously destabilizing the ends of the tube but also restricting the available motion leading to faster processes.

When considering this effect, it is necessary to take into account the impact of increased temperature of the bound sequences relative to the free ones when comparing dynamic timescales.[31] This may play a role in the apparent acceleration of the dynamics. However, previous studies have indicated only a modest linear correlation between the rate of the nanosecond processes and T_0.[30,31] Indeed, analysis of the impact of T_0 on the observed dynamics in our experiments show that τ_1 is relatively insensitive to temperature, consistent with a process that does not involve the crossing of a large energy barrier and suggesting a rugged potential energy surface for the dsDNA. This is also in keeping with previous observations for RNA[36] and DNA.[34,31] It is also interesting to note that the faster dynamics (τ_1) show slightly more stretched behavior than the slower dynamics. This could arise from the narrowing of the temperature distribution in the cell but may also indicate behavior consistent with traversing a rugged energy landscape.[50] In contrast, Arrhenius-type behavior was reported for the full melting transition.[31] Unfortunately, the shorter duration of our T-jump (1 ms) in comparison to the melting dynamics of the complexes precludes a thorough analysis of the T_0 dependence of τ_2 for the bound sequences. Decreasing T_0 for the free sequences was found to reduce the amplitude of the melting portion of the time trace in a systematic manner (Figure S7) consistent with slower kinetics further from the transition temperature as would be expected. Indeed, this behavior closely mimics the observations seen for melting of the complexes and further reinforces the assignment of suppressed T-jump signal amplitude to slower melting dynamics.

CONCLUSIONS

Employing ultrafast time-resolved infrared spectroscopy using nanosecond T-jump initiation to study the melting of double stranded (ds)DNA oligomers in the presence and absence of minor groove binding ligand Hoechst 33258 shows that ligand binding to A-tract DNA results in a dramatic increase in the timescales for strand melting from 30 to ~250 μs. Ligand binding also leads to suppression of premelting disruption of the dsDNA structure, including end-fraying, which takes place on 100 ns timescales. Comparison of results for the A-tract sequence with a sequence featuring an alternating AT binding region results in a less dramatic slowing down of the melting process and limited suppression of premelting sequence perturbation and end-fraying. These results demonstrate a dynamic impact of the ligand on the DNA sequence that correlates with binding strength and thermodynamic stabilization of the duplex structure. The results also show that ligand binding remotely influences the dynamic behavior of base pairs outwith the main binding site, suggesting potential dynamic origins of allosteric communication mechanisms in dsDNA.

■ ASSOCIATED CONTENT

ⓢ Supporting Information

The Supporting Information is available free of charge on the ACS Publications website at DOI: 10.1021/acs.jpcb.9b04354.

> Additional details on experimental and data preprocessing methods; additional IR absorption and T-jump data as described in the text (PDF)

■ AUTHOR INFORMATION

Corresponding Author

*E-mail: neil.hunt@york.ac.uk.

ORCID ⓞ

Neil T. Hunt: 0000-0001-7400-5152

Notes

The authors declare no competing financial interest.

■ REFERENCES

(1) Erwin, G. S.; Grieshop, M. P.; Ali, A.; Qi, J.; Lawlor, M.; Kumar, D.; Ahmad, I.; McNally, A.; Teider, N.; Worringer, K.; Sivasankaran, R.; et al. Synthetic transcription elongation factors license transcription across repressive chromatin. *Science* **2017**, *358*, 1617−1622.

(2) Singh, I.; Wendeln, C.; Clarke, A. W.; Cooper, J. M.; Ravoo, B. J.; Burley, G. A. Sequence-selective detection of double-stranded DNA sequences using pyrrole-imidazole polyamide microarrays. *J. Am. Chem. Soc.* **2013**, *135*, 3449−3457.

(3) Krpetić, Ž.; Singh, I.; Su, W.; Guerrini, L.; Faulds, K.; Burley, G. A.; Graham, D. Directed assembly of DNA-functionalized gold nano-particles using pyrrole-imidazole polyamides. *J. Am. Chem. Soc.* **2012**, *134*, 8356−8359.

(4) Su, W.; Schuster, M.; Bagshaw, C. R.; Rant, U.; Burley, G. A. Site-specific assembly of DNA-based photonic wires by using programmable polyamides. *Angew. Chem., Int. Ed.* **2011**, *50*, 2712−2715.

(5) Dervan, P. B.; Edelson, B. S. Recognition of the DNA minor groove by pyrrole-imidazole polyamides. *Curr. Opin. Struct. Biol.* **2003**, *13*, 284−299.

(6) Chenoweth, D. M.; Dervan, P. B. Allosteric modulation of DNA by small molecules. *Proc. Natl. Acad. Sci.* **2009**, *106*, 13175−13179.

(7) Parkinson, J. A.; Scott, F. J.; Suckling, C. J.; Wilson, G. Exceptionally strong intermolecular association in hydrophobic DNA minor groove binders and their potential therapeutic consequences. *Med. Chem. Commun.* **2013**, *4*, 1105−1108.

(8) Rohs, R.; Jin, X.; West, S. M.; Joshi, R.; Honig, B.; Mann, R. S. Origins of specificity in protein-DNA recognition. *Annu. Rev. Biochem.* **2010**, *79*, 233−269.

(9) Bueren-Calabuig, J. A.; Giraudon, C.; Galmarini, C. M.; Egly, J. M.; Gago, F. Temperature-induced melting of double-stranded DNA in the absence and presence of covalently bonded antitumour drugs: insight from molecular dynamics simulations. *Nucleic Acids Res.* **2011**, *39*, 8248−8257.

(10) Duboué-Dijon, E.; Fogarty, A. C.; Hynes, J. T.; Laage, D. Dynamical disorder in the DNA hydration shell. *J. Am. Chem. Soc.* **2016**, *138*, 7610−7620.

(11) Pal, S.; Maiti, P. K.; Bagchi, B.; Hynes, J. T. Multiple time scales in solvation dynamics of DNA in aqueous solution: The role of water, counterions, and cross-correlations. *J. Phys. Chem. B* **2006**, *110*, 26396−26402.

(12) Furse, K. E.; Corcelli, S. A. The dynamics of water at DNA interfaces: Computational studies of Hoechst 33258 bound to DNA. *J. Am. Chem. Soc.* **2008**, *130*, 13103−13109.

(13) Guchhait, B.; Liu, Y.; Siebert, T.; Elsaesser, T. Ultrafast vibrational dynamics of the DNA backbone at different hydration levels mapped by two-dimensional infrared spectroscopy. *Struct. Dyn.* **2016**, *3*, 043202.

(14) Siebert, T.; Guchhait, B.; Liu, Y.; Costard, R.; Elsaesser, T. Anharmonic backbone vibrations in ultrafast processes at the DNA-water interface. *J. Phys. Chem. B* **2015**, *119*, 9670−9677.

(15) Yang, M.; Szyc, Ł.; Elsaesser, T. Decelerated water dynamics and vibrational couplings of hydrated DNA mapped by two-dimensional infrared spectroscopy. *J. Phys. Chem. B* **2011**, *115*, 13093−13100.

(16) Szyc, Ł.; Yang, M.; Elsaesser, T. Ultrafast energy exchange via water-phosphate interactions in hydrated DNA. *J. Phys. Chem. B* **2010**, *114*, 7951−7957.

(17) Floisand, D. J.; Corcelli, S. A. Computational study of phosphate vibrations as reporters of DNA hydration. *J. Phys. Chem. Lett.* **2015**, *6*, 4012−4017.

(18) González-Jiménez, M.; Ramakrishnan, G.; Harwood, T.; Lapthorn, A. J.; Kelly, S. M.; Ellis, E. M.; Wynne, K. Observation of coherent delocalized phonon-like modes in DNA under physiological conditions. *Nat. Commun.* **2016**, *7*, 11799.

(19) Hithell, G.; Shaw, D. J.; Donaldson, P. M.; Greetham, G. M.; Towrie, M.; Burley, G. A.; Parker, A. W.; Hunt, N. T. Long-range vibrational dynamics are directed by Watson−Crick base pairing in duplex DNA. *J. Phys. Chem. B* **2016**, *120*, 4009−4018.

(20) Krummel, A. T.; Zanni, M. T. DNA vibrational coupling revealed with two-dimensional infrared spectroscopy: Insight into why vibrational spectroscopy is sensitive to DNA structure. *J. Phys. Chem. B* **2006**, *110*, 13991−14000.

(21) Krummel, A. T.; Mukherjee, P.; Zanni, M. T. Inter and intrastrand vibrational coupling in DNA studied with heterodyned 2D-IR spectroscopy. *J. Phys. Chem. B* **2003**, *107*, 9165−9169.

(22) Peng, C. S.; Jones, K. C.; Tokmakoff, A. Anharmonic vibrational modes of nucleic acid bases revealed by 2D IR spectroscopy. *J. Am. Chem. Soc.* **2011**, *133*, 15650−15660.

(23) Hithell, G.; Donaldson, P. M.; Greetham, G. M.; Towrie, M.; Parker, A. W.; Burley, G. A.; Hunt, N. T. Effect of oligomer length on vibrational coupling and energy relaxation in double-stranded DNA. *Chem. Phys.* **2018**, *512*, 154−164.

(24) Hithell, G.; González-Jiménez, M.; Greetham, G. M.; Donaldson, P. M.; Towrie, M.; Parker, A. W.; Burley, G. A.; Wynne, K.; Hunt, N. T. Ultrafast 2D-IR and optical Kerr effect spectroscopy reveal the impact of duplex melting on the structural dynamics of DNA. *Phys. Chem. Chem. Phys.* **2017**, *19*, 10333−10342.

(25) Ramakers, L. A.; Hithell, G.; May, J. J.; Greetham, G. M.; Donaldson, P. M.; Towrie, M.; Parker, A. W.; Burley, G. A.; Hunt, N. T. 2D-IR spectroscopy shows that optimized DNA minor groove binding of Hoechst33258 follows an induced fit model. *J. Phys. Chem. B* **2017**, *121*, 1295−1303.

(26) Ranjan, N.; Story, S.; Fulcrand, G.; Leng, F. F.; Ahmad, M.; King, A.; Sur, S.; Wang, W. D.; Tse-Dinh, Y. C.; Arya, D. P. Selective inhibition of Escherichia coli RNA and DNA topoisomerase I by

Hoechst 33258 derived mono- and bisbenzimidazoles. *J. Med. Chem.* **2017**, *60*, 4904−4922.

(27) Harshman, K. D.; Dervan, P. B. Molecular recognition of B-DNA by Hoechst 33258. *Nucleic Acids Res.* **1985**, *13*, 4825−4835.

(28) Bazhulina, N. P.; Nikitin, A. M.; Rodin, S. A.; Surovaya, A. N.; Kravatsky, Y. V.; Pismensky, V. F.; Archipova, V. S.; Martin, R.; Gursky, G. V. Binding of Hoechst 33258 and its derivatives to DNA. *J. Biomol. Struct. Dyn.* **2009**, *26*, 701−718.

(29) Fornander, L. H.; Wu, L.; Billeter, M.; Lincoln, P.; Nordén, B. Minor-groove binding drugs: Where is the second Hoechst 33258 molecule? *J. Phys. Chem. B* **2013**, *117*, 5820−5830.

(30) Rahimian, M.; Miao, Y.; Wilson, W. D. Influence of DNA structure on adjacent site cooperative binding. *J. Phys. Chem. B* **2008**, *112*, 8770−8778.

(31) Kiser, J. R.; Monk, R. W.; Smalls, R. L.; Petty, J. T. Hydration changes in the association of Hoechst 33258 with DNA. *Biochemistry* **2005**, *44*, 16988−16997.

(32) Loontiens, F. G.; Regenfuss, P.; Zechel, A.; Dumortier, L.; Clegg, R. M. Binding characteristics of Hoechst 33258 with calf thymus DNA, poly[d(A-T)] and d(CCGGAATTCCGG): multiple stoichiometries and determination of tight binding with a wide spectrum of site affinities. *Biochemistry* **1990**, *29*, 9029−9039.

(33) Bostock-Smith, C. E.; Harris, S. A.; Laughton, C. A.; Searle, M. S. Induced fit DNA recognition by a minor groove binding analogue of Hoechst33258: Fluctuations in DNA A-tract structure investigated by NMR and molecular dynamics simulations. *Nucleic Acids Res.* **2001**, *29*, 693−702.

(34) Narayanan, R.; Zhu, L.; Velmurugu, Y.; Roca, J.; Kuznetsov, S. V.; Prehna, G.; Lapidus, L. J.; Ansari, A. Exploring the energy landscape of nucleic acid hairpins using laser temperature-jump and microfluidic mixing. *J. Am. Chem. Soc.* **2012**, *134*, 18952−18963.

(35) Kuznetsov, S. V.; Sugimura, S.; Vivas, P.; Crothers, D. M.; Ansari, A. Direct observation of DNA bending/unbending kinetics in complex with. DNA-bending protein IHF. *Proc. Nat. Acad. Sci.* **2006**, *103*, 18515−18520.

(36) Stancik, A. L.; Brauns, E. B. Rearrangement of partially ordered stacked conformations contributes to the rugged energy landscape of a small RNA hairpin. *Biochemistry* **2008**, *47*, 10834−10840.

(37) Brauns, E. B.; Dyer, R. B. Time-resolved infrared spectroscopy of RNA folding. *Biophys. J.* **2005**, *89*, 3523−3530.

(38) Sanstead, P. J.; Stevenson, P.; Tokmakoff, A. Sequence-dependent mechanism of DNA oligonucleotide dehybridization resolved through infrared spectroscopy. *J. Am. Chem. Soc.* **2016**, *138*, 11792−11801.

(39) Sanstead, P. J.; Tokmakoff, A. Direct observation of activated kinetics and downhill dynamics in DNA dehybridization. *J. Phys. Chem. B* **2018**, *122*, 3088−3100.

(40) Greetham, G. M.; Sole, D.; Clark, I. P.; Parker, A. W.; Pollard, M. R.; Towrie, M. Time-resolved multiple probe spectroscopy. *Rev. Sci. Instrum.* **2012**, *83*, 103107.

(41) Greetham, G. M.; Donaldson, P. M.; Nation, C.; Sazanovich, I. V.; Clark, I. P.; Shaw, D. J.; Parker, A. W.; Towrie, M. A 100 kHz Time-resolved multiple-probe femtosecond to second Infrared absorption spectrometer. *Appl. Spectrosc.* **2016**, *70*, 645−653.

(42) Fritzsch, R.; Donaldson, P. M.; Greetham, G. M.; Towrie, M.; Parker, A. W.; Baker, M. J.; Hunt, N. T. Rapid screening of DNA-ligand complexes via 2D-IR spectroscopy and ANOVA-PCA. *Anal. Chem.* **2018**, *90*, 2732−2740.

(43) Lee, C.; Cho, M. Vibrational dynamics of DNA : IV. Vibrational spectroscopic characteristics of A-, B-, and Z-form DNA's. *J. Chem. Phys.* **2007**, *126*, 145102.

(44) Lee, C.; Park, K.-H.; Kim, J.-A.; Hahn, S.; Cho, M. Vibrational dynamics of DNA. III. Molecular dynamics simulations of DNA in water and theoretical calculations of the two-dimensional vibrational spectra. *J. Chem. Phys.* **2006**, *125*, 114510.

(45) Lee, C.; Park, K.-H.; Cho, M. Vibrational dynamics of DNA. I. Vibrational basis modes and couplings. *J. Chem. Phys.* **2006**, *125*, 114508.

(46) Lee, C.; Cho, M. Vibrational dynamics of DNA. II. Deuterium exchange effects and simulated IR absorption spectra. *J. Chem. Phys.* **2006**, *125*, 114509.

(47) Greetham, G. M.; Clark, I. P.; Fritzsch, R.; Minnes, L.; Hunt, N. T.; Towrie, M. Time-resolved temperature-jump infrared spectroscopy at high repetition-rate. *Rev Sci Instrum* **2019,** *in revision*.

(48) Doorley, G. W.; Wojdyla, M.; Watson, G. W.; Towrie, M.; Parker, A. W.; Kelly, J. M.; Quinn, S. J. Tracking DNA excited states by picosecond-time-resolved infrared spectroscopy: Signature band for a charge-transfer excited state in stacked adenine−thymine systems. *J. Phys. Chem. Lett.* **2013**, *4*, 2739−2744.

(49) Gotoh, O.; Tagashira, Y. Stabilities of nearest-neighbor doublets in double-helical DNA determined by fitting calculated melting profiles to observed profiles. *Biopolymers* **1981**, *20*, 1033−1042.

(50) Hamm, P.; Helbing, J.; Bredenbeck, J. Stretched versus compressed exponential kinetics in α-helix folding. *Chem. Phys.* **2006**, *323*, 54−65.